Catalysis Today 171 (2011) 211–220

Contents lists available at ScienceDirect

Catalysis Today

journal homepage: www.elsevier.com/locate/cattod

Methane conversion to light olefins—How does the methyl halide route differ from the methanol to olefins (MTO) route?

Unni Olsbye[a,*], Ole Vaaland Saure[a], Naresh Babu Muddada[a,b], Silvia Bordiga[b], Carlo Lamberti[b], Merete Hellner Nilsen[a], Karl Petter Lillerud[a], Stian Svelle[a]

[a] inGAP Centre of Research Based Innovation, Department of Chemistry, University of Oslo, P.O. Box 1033, Blindern, N-0315 Oslo, Norway
[b] Department of Inorganic, Physical and Materials Chemistry and NIS Centre of Excellence, University of Torino, Via P. Giuria 7, I-0125 Torino, Italy

ARTICLE INFO

Article history:
Available online 14 June 2011

Keywords:
Methyl chloride to olefins
MeXTO
MTO
SAPO-34
Reaction mechanism
Spectroscopy
Acid catalysis

ABSTRACT

The methyl halide to hydrocarbons (MeXTH) reaction represents the second step in a potential two-step route from methane to light olefins or gasoline-range hydrocarbon mixtures. In this contribution, the methyl chloride to olefins reaction (MeXTO) was studied over a H-SAPO-34 catalyst with (Al + P)/Si = 19 by means of catalytic testing at 350–400 °C and WHSV = 11.7 h^{-1}, infrared spectroscopy and isotopic labelling experiments. Only minor degradation of the H-SAPO-34 material was observed by X-Ray diffraction or infrared spectroscopy after 5 sequential test-regeneration cycles at 400 °C and 550 °C, respectively. Co-feed experiments using ^{13}C-methyl chloride and ^{12}C-ethene or ^{12}C-propene at 400 °C indicated that the conversion level of each compound is directly related to its proton affinity. Furthermore, under the conditions used, no inhibitive effect of the alkenes on methyl chloride conversion was observed. Transient isotopic labelling experiments suggested that hexamethyl benzene is an important reaction intermediate in alkene formation from methyl chloride. However, the isotopic labelling of effluent products during ^{13}C-methyl chloride–^{12}C-alkene co-feed experiments suggested that alkene methylation and interconversion reactions may contribute significantly to C_3^+ formation. The findings are in general agreement with similar studies of the methanol to olefins reaction over the same catalyst topology.

1. Introduction

Depleting oil reserves, combined with an improved ability for exploitation of remote natural gas [1], has recently boosted the interest for use of natural gas as energy source and as feedstock for the petrochemical industry.

Today, industrial processes based on methane, the main component of natural gas, proceed via synthesis gas (syngas; CO and H_2) production. In an oxidative atmosphere, using O_2, H_2O or CO_2 as the oxidant, syngas is the thermodynamically favoured product from methane at high temperatures [2]. Syngas production therefore circumvents the kinetic selectivity challenges of methane conversion, but at the expense of high construction costs. Wilhelm et al. recently reported that the syngas facility represents 50% of the construction costs for a gas-to-liquids (GTL) plant [3].

Huge efforts have been devoted to the development of alternative, direct conversion routes from methane to petrochemical products over the past 3 decades (see e.g. [4,5] and references therein). However, methane is a symmetrical, non-polar molecule, and functionalisation of that molecule by breaking a C–H bond unavoidably introduces asymmetry, thus increasing the probability of further reaction. The conversion–selectivity relationship for some direct methane conversion routes, found in Refs. [4–10] is reproduced in Fig. 1.

$$A \xrightarrow{k_1} B \xrightarrow{k_2} C \quad (1)$$

Consider a sequential reaction scheme with first order reactions (Eq. (1)). A comparison between the literature data and a simulated conversion–selectivity plot for Eq. (1) with $k_2 = k_1$ show that for two of the most-studied processes; ethene formation by the oxidative coupling of methane (OCM) [5], as well as direct methanol or formaldehyde production from methane via catalytic partial oxidation [4]; the selectivity versus conversion plots lie at or below the $k_2 = k_1$ trend-line, implying that $k_2 \geq k_1$ (Fig. 1). The same is true for MeCl formation from methane in gas phase or over $LaCl_3$-based catalysts [6,7], while the use of super-acids as catalysts have been reported to give high yields of MeCl and MeBr from methane [8,9]. Furthermore, MeBr formation is thermodynamically favoured over CH_2Br_2, leading to the high MeBr yields reported for gas phase formation of MeBr from methane and Br_2 [10]. Methyl halides thus appear as promising intermediates for non-syngas methane conversion.

* Corresponding author. Tel.: +47 22 85 54 56; fax: +47 22 85 54 41.
E-mail address: unni.olsbye@kjemi.uio.no (U. Olsbye).

0920-5861/$ – see front matter © 2011 Elsevier B.V. All rights reserved.
doi:10.1016/j.cattod.2011.04.020

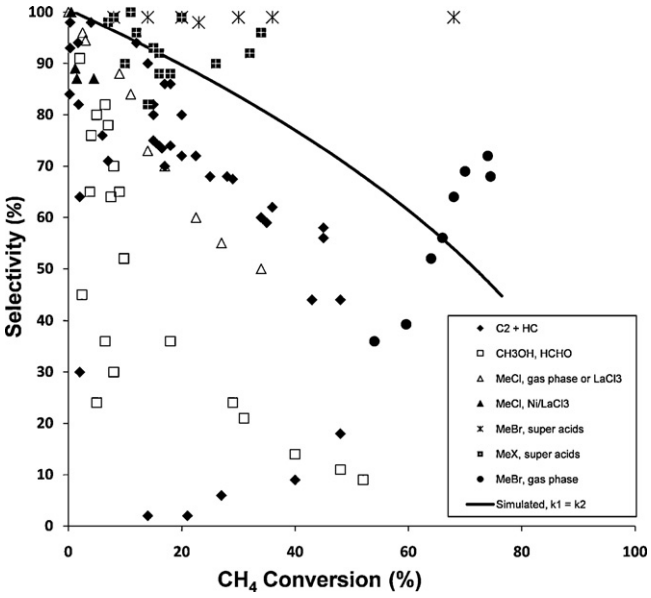

Fig. 1. Conversion–selectivity plot for direct methane conversion routes. Data from [4–10] and references therein.

A methyl halide to hydrocarbons process (MeXTH) was patented by Taylor and coworkers during the 1980s [11–13]. The process was conducted over a H-ZSM-5 catalyst, with global reaction scheme:

$$n\mathrm{CH_3X} \rightarrow \mathrm{C}_n\mathrm{H}_{2n} + n\mathrm{HCl} \quad (2)$$

H-ZSM-5 is a Brønsted acidic zeolite with MFI topology, in which straight and sinusoidal 10-ring channels compose a 3D channel network with 5.1×5.5 and 5.3×5.6 Å pore diameter. This catalyst produces a gasoline-range product spectrum ranging from C_2–C_4 alkenes and alkanes, up to C_{10} aromatics (methylated benzenes) (Fig. 2, bottom) from MeCl. Later, Su and coworkers [14–17] and Olsbye and coworkers [18,19] have explored the potential of zeotypes with chabasite structure (H-SAPO-34 with and without bivalent metal substitution) as catalysts for the methyl halide to hydrocarbons process. H-SAPO-34 is a Brønsted acidic zeotype with CHA topology, which is composed of double 6-rings which are stacked in an ABC pattern. This stacking leads to a 3-dimensional 8-ring channel structure with cavities at channel intersections. The cavity window diameter is 3.8×3.8 Å and the cavity diameter is 7.3 Å × 12 Å. Due to the narrow cavity openings, this topology yields a product spectrum rich in light, linear alkenes (Fig. 2, top).

The above-mentioned studies concluded that the methyl halide to hydrocarbons reaction bears strong resemblance to the more studied methanol to hydrocarbons reaction (MTH), with global reaction scheme:

$$n\mathrm{CH_3OH} \rightarrow \mathrm{C}_n\mathrm{H}_{2n} + n\mathrm{H_2O} \quad (3)$$

The MTH reaction is part of the conventional methane conversion scheme, i.e. methanol may be produced from syngas.

The mechanism of the MTH reaction has been extensively studied since its discovery in 1977 [20]. Although several direct reaction mechanisms were initially proposed, there is now general consensus about the so-called "hydrocarbon pool" mechanism, initially proposed by Dahl and Kolboe, in which methyl groups are constantly added to the pool by reaction with methanol, and alkenes are subsequently split off [21–23]. Independent research by several groups points to multiply methylated benzene molecules, hereinafter called polymethylbenzenes (polyMBs), as main intermediates in the MTH reaction over wide-pore zeolites and zeotypes, such as H-SAPO-34 [24–40]. The active site is thus not the Brönsted acid site alone, but an organic–inorganic hybrid material consisting

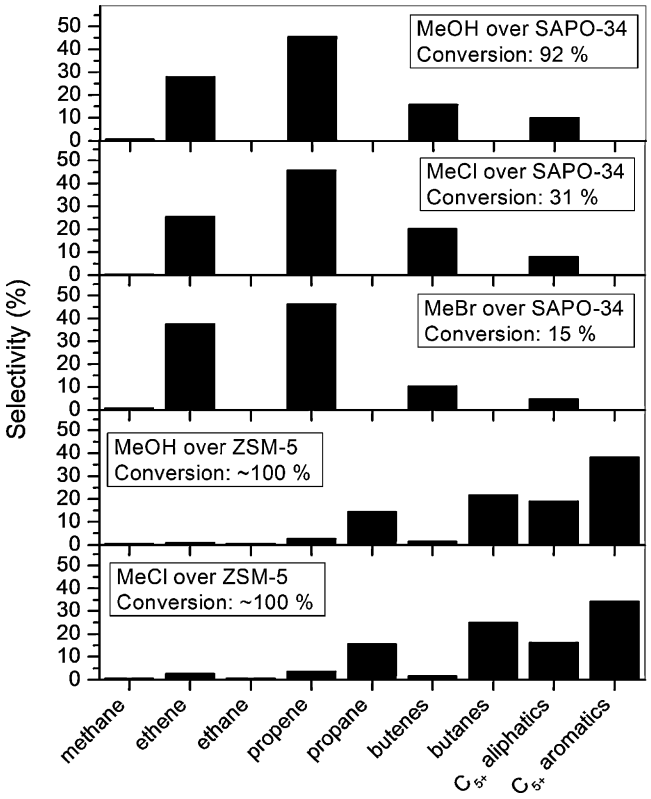

Fig. 2. Product selectivities for the conversion of methanol or methyl halides at 350 °C over H-SAPO-34 (top) and H-ZSM-5 (bottom). Data are taken from [13,18].

of a proton in close interaction with a polyMB molecule. Alkenes may be produced by formation of a polymethylbenzenium ion, which splits off alkenes, leaving behind a lower polyMB analogue which is subsequently methylated back to its higher analogue, thereby completing the catalytic cycle.

Among the similarities between MTH and MeXTH is the product selectivity of the two processes. The effluent composition of the MTH and MeXTH (X = Cl, Br) processes over H-SAPO-34 and H-ZSM-5 under similar reaction conditions is shown in Fig. 2. For H-ZSM-5, both processes were carried out under conditions giving full conversion (350 °C, WHSV = 1 h^{-1}). As may be observed in Fig. 2, the product composition is very similar for the two processes, giving hydrocarbons ranging from C_2–C_4 alkenes and alkanes, up to C_{10} aromatics (methylated benzenes). For H-SAPO-34, care was taken to carry out the study at less than 100% conversion. Before testing, the catalysts were activated by a propene pulse, in order for the catalyst's active (hybride) sites to be similar when converting the various reactants [18]. It is worth noting that, in spite of the similar product pattern, giving mainly C_2–C_4 alkenes, the conversion level of the methyl halides was much inferior to that of methanol, i.e.; 5.2% MeCl conversion, 3.9% MeBr conversion, and 92% MeOH conversion, at zero time on stream at 350 °C, P(MeX) ~ 0.1 bar and WHSV = 6.2–7.7 h^{-1}. When decreasing the WHSV of the methyl halide feed to 0.8 h^{-1}, the MeCl and MeBr conversions were still inferior to that of methanol at the higher WHSV, i.e., 31% and 15%, respectively. The product selectivity from the methyl halides was very close to that observed for methanol conversion (Fig. 2, top). The similar selectivity patterns observed are in line with recent evidence that product selectivity in MTH over H-SAPO-34 is governed by product shape selectivity [41].

In the present contribution, our aim was to further explore the potential of the methyl chloride to olefins process. In particular, we wanted to elucidate the reason for the lower conversion

of methyl chloride versus methanol observed under similar reaction conditions [18]. Literature reports suggest that the lower MeCl conversion is due to either a lower proton affinity of methyl chloride compared to methanol (647 kJ/mol versus 754 kJ/mol, respectively [42]), leading to a lower coverage of active sites by adsorbed MeCl and thus a lower rate of subsequent methylation reactions [43]; to competitive adsorption of alkene products [18] or to deterioration of the acid sites by HCl formed in the MeXTH reaction [15,17]. A fourth possibility may be that methanol and methyl chloride are converted via different reaction intermediates.

In the following, each of these hypotheses will be explored by using various techniques, including catalytic testing, infrared spectroscopy and isotopic labelling experiments.

2. Experimental

2.1. Catalyst preparation and characterization

H-SAPO-34 was synthesized using tetramethylammonium hydroxide (TEA) as the structure directing agent. The molar composition of the synthesis gel was $1.0TEA_2O{:}1.0Al_2O_3{:}0.3SiO_2{:}0.89HCl{:}0.89P_2O_5{:}64H_2O$ according to a previously reported procedure [44,45]. The protonated sample was obtained by calcination of the as prepared material at 550 °C and submitted to characterization using powder X-ray diffraction (XRD), scanning electron microscopy (SEM), N_2 porosimetry, NH_3 TPD and infrared spectroscopy with CO or HCl adsorption. Powder XRD patterns were recorded on a Siemens D5000 diffractometer using Cu $K_{\alpha 1}$ radiation ($\lambda = 1.541$ Å). The crystal morphology and particle size was investigated with a SEM FEI Quanta 200 FEG-ESEM with EDS. A thin layer of catalyst was retained on a sample holder with double sided carbon tape by sprinkling the powder on top. Both backscatter and Evert-Thornley detectors were used. Transmission FTIR spectroscopy was performed using a Bruker Vertex 80 FTIR spectrometer with MCT detector. The measurements were performed at 2 cm^{-1} resolution on self supporting wafers. Before the measurements, the sample was oxidized and subsequently outgassed at 500 °C for 2 h. CO was dosed from a vacuum line permanently attached to the IR cell kept at −203 °C. High-purity HCl was produced by reaction of H_2 with optical AgCl at 973 K and used after elimination of residual H_2 through repeated freezing cycles, by using a cold trap kept at 77 K [46,47]. HCl in the gas phase was put in a closed reservoir and dosed at room temperature on the activated zeolite. The zeolite sample was then treated in a closed cell at 400 °C for 30 min and the final IR spectrum has been recorded after pumping at room temperature.

2.2. Catalytic testing

Catalytic tests were carried out in a tubular quartz fixed-bed reactor of 9 mm i.d. The temperature in the catalyst bed was measured by a thermocouple (Newport Omega) centered axially inside the reactor. Before testing, the catalyst (typically 100 mg of 0.25–0.42 mm particles, diluted with 100 mg of 0.25–0.42 mm quartz particles) was heated to 500 °C in an Ar stream and cooled to the reaction temperature (350 or 400 °C) before switching to the feed; typically CH_3Cl (9.5 N ml/min) diluted in helium (5 N ml/min) resulting in a weight hourly space velocity, WHSV = 11.7 h^{-1}.

Reactant conversion and product selectivities were measured with a Carlo-Erba 6000 Gas Chromatograph with a JW GS-GasPro column (60 m × 0.32 mm) and a flame ionization detector (FID).

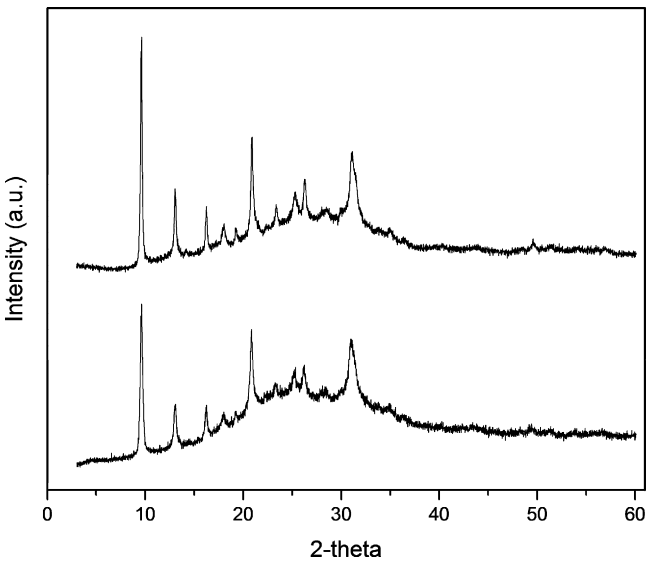

Fig. 3. X-Ray diffractogram (XRD) of H-SAPO-34 before (top) and after (bottom) 5 test – regeneration cycles at 400 °C and 550 °C, respectively.

2.3. Isotopic labelling experiments

Isotopic labelling experiments were performed at 400 °C over H-SAPO-34 (100 mg of 0.25–0.42 mm particle size). Transient isotopic labelling experiments were performed by using two parallel feed lines, one in which He (5 N ml/min) was mixed with ^{12}C-MeCl (10 N ml/min), and another in which He (5 N ml/min) was mixed with ^{13}C-MeCl (10 N ml/min), and rapidly switching between them. Co-feed experiments were performed by premixing ^{13}C-MeCl (10 N ml/min) with either ^{12}C-ethene (5 N ml/min) or ^{12}C-propene (3.3 N ml/min), thus obtaining a ^{12}C:^{13}C ratio of 1:1 in both cases, and diluting the gas with He (10 N ml/min).

Isotopic composition of the gas-phase products was determined from effluent analyses carried out using an HP 6890/HP 5973 GC–MS equipped with a JW GS-GasPro column (60 m × 0.32 mm). The computational method used for determining the isotope content and distribution in ^{12}C/^{13}C compounds has been outlined previously [48,49]. Conversion of methyl chloride and ethene or propene was calculated by comparing their relative abundances in

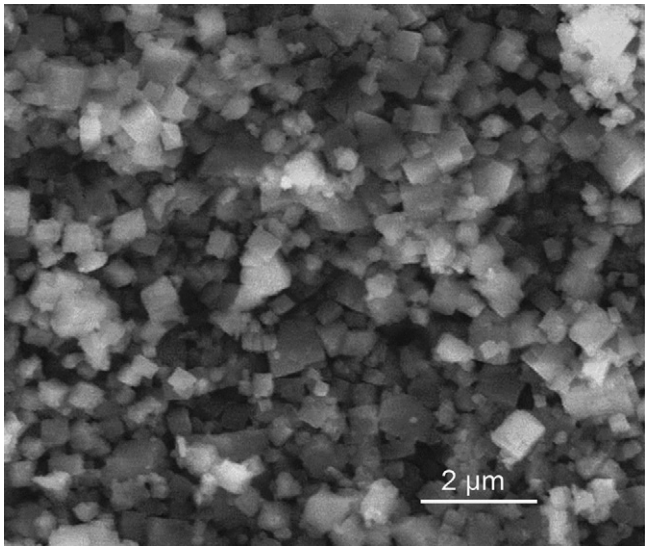

Fig. 4. Scanning electron microscopy (SEM) image of H-SAPO-34.

the feed and effluent, respectively. During ethene co-feed experiments, only unlabelled ethene was considered unconverted, while $^{13}C_1$- and $^{13}C_2$-labelled ethene were considered as reaction product. Propene conversion was calculated accordingly during propene co-feed experiments.

2.4. Analysis of organics retained in the pores of the catalyst

In order to obtain detailed information about the identity and isotopic composition of the compounds trapped inside the pores of the catalysts after a catalytic reaction, the spent catalyst (typically 15 mg) was dissolved in 15% hydrofluoric acid (HF, 1 ml) and the organic compounds were extracted with CH_2Cl_2 (1 ml). The organic phase and the water phase were separated and the CH_2Cl_2 extract was analyzed by gas chromatography–mass spectrometry (GC–MS) using an HP 6890/HP 5973 instrument with a HP-5MS column (60 m × 250 μm × 0.25 μm). This technique for dissolving spent catalyst in HF to liberate the trapped aromatics has been described previously in more detail [31,50].

3. Results

3.1. Catalyst characterization

The X-ray diffractogram of H-SAPO-34 indicated that the sample contained CHA as the only crystalline phase (Fig. 3). A SEM image of the catalyst is shown in Fig. 4. The sample consisted of cubic crystals in the size range 0.5–2 microns. N_2 porosimetry (not shown) revealed that the catalyst was purely microporous, and did not contain mesopores. The specific surface area of the material, calculated according to the BET method, was 447 m^2/g. Integration of the NH_3–TPD curve (not shown) indicated a (Al + P)/Si ratio of 19, which corresponds to an average of one acid site per 1.5 cavities in the CHA structure.

Infrared (IR) spectra for the fresh and used catalyst, oxidized and subsequently outgassed at 500 °C for 2 h, are compared in Fig. 5. The doublet, typical of Brønsted O–H sites expected in case of standard H-SAPO-34 is observed at 3627 cm^{-1} and 3603 cm^{-1} and it is very similar in case of both samples (the difference is less than 20% of the total). Minor features at 3752, 3743 and 3677 cm^{-1} correspond to Al–OH, Si–OH and P–OH, respectively (Fig. 5 top, left). Upon CO adsorption, the frequency of the main peak was shifted to approx. 3357 cm^{-1}, with a shoulder at 3440 cm^{-1}. The shift, which is proportional to the acid strength of the material, $\Delta\nu \sim 270\ cm^{-1}$, is typical for H-SAPO-34 [51]. In the CO stretch frequency range (Fig. 5 top, right), a main feature due to CO adsorbed on Brønsted acidic sites was observed at 2173 cm^{-1}, slightly moving to 2170 cm^{-1} at higher CO pressure. This component is slightly more intense in case of the fresh sample than for used zeolite. The band at 2140 cm^{-1} is due to condensed CO. No peaks were observed in the range typical of Lewis acid sites, i.e. around 2230 cm^{-1} [52].

3.2. Influence of HCl treatment

It has previously been shown that HCl, either fed alone or formed from CH_3Cl at elevated temperatures, may induce Al–O–P bond breaking in H-SAPO-34 [15,17]. HCl adsorption was therefore performed in the present work, in order to verify this effect in the material used here.

Infrared spectra obtained for H-SAPO-34 before and after HCl dosage are shown in Fig. 6. The bottom, black spectrum corresponds to the untreated H-SAPO-34 sample activated in high vacuo, and is identical to the spectrum shown in Fig. 5 (top left).

The blue curve (Fig. 6, top) shows the effect of interaction with HCl at room temperature. The curve was obtained after subtraction of the background spectrum. The main features are:

(a) No substantial change is observed for the component at 3752 cm^{-1} associated to Si–OH.
(b) Growth of an intense band at 3674 cm^{-1} associated to *P–OH* species is observed. The appearance of this feature suggests that upon interaction with HCl, *Al–O–P* bonds are hydrolysed to form *Al–Cl* and *P–OH* species. Unfortunately, no direct evidence of *Al–Cl* formation could be obtained, as this band presumably falls below 400 cm^{-1}.
(c) Bands associated to strong Brønsted sites are significantly eroded (negative complex band with minimum at 3628 cm^{-1} and a shoulder at 3600 cm^{-1}). This result implies that both sites are engaged in H-bonds with HCl. At lower frequency, extending till below 1000 cm^{-1}, we observe in fact the growth of a complex absorption due to the formation of H-bonded adducts. Maxima at 3338, 2440 and at 1620 cm^{-1} are observed. Centered at 2880 cm^{-1}, HCl in gas phase is present.

The red curve (Fig. 6 top) illustrates the effect of heating at 400 °C for 30 min in a closed cell after admittance of HCl, and subsequent outgassing at room temperature (RT).

The curve was obtained after subtraction of the background spectrum. The main features are:

(a) Appearance of a weak band at 3752 cm^{-1} indicating a small increase of Si–OH species.
(b) Further increase of the band at 3675 cm^{-1} associated to *P–OH* species. This result indicates an irreversible modification of the zeolitic structure.
(c) Distinct maxima at 3470, 2890, 2460 and 1606 cm^{-1} appear on an extensive and intense absorption extending till below 1000 cm^{-1}. This peculiar spectrum is due to the formation of a complex mixture of species characterized by medium and strong H-bonds. In particular, we expect that strong Brønsted sites (*–Si(OH)Al–*), forming "*O–H···Cl–H*" adducts, are responsible of strong H-bonds. It is well known that stretching mode [ν(OH)] of strong H-bonded OH groups is "modulated" by Fermi resonance effects caused by its combination with upward shifted 2δ(OH) and 2γ(OH) modes of the same species. This complex phenomenon causes the appearance of three maxima at 2890, 2460 and 1627 cm^{-1} labelled as A, B and C components. In this case A and B components have similar intensities, while C components play a minor role. Finally, we expect also the formation of "*P–O–H···Cl–H*" adducts that should be characterized by medium strength H-bonds; probably the band at 3470 cm^{-1} is associated to this species.

These findings are in general agreement with data reported by Su and coworkers for HCl adsorption on a H-SAPO-34 sample [15]. They definitely show that HCl reacts strongly with the zeolitic matrix. However, it is also clear that all the changes do not compromize the crystallinity of the material (Fig. 3) and are mostly reversible, as documented by the nearly total restoration of the OH groups upon activation (Fig. 5).

3.3. Catalytic activity and conversion capacity

Fig. 7 shows the methyl chloride conversion versus time on stream over H-SAPO-34 at 350–400 °C. An increase in initial conversion, as well as a more rapid induction and deactivation, is observed with increasing temperature. Product selectivities versus time on stream at two temperatures are shown in Supporting information,

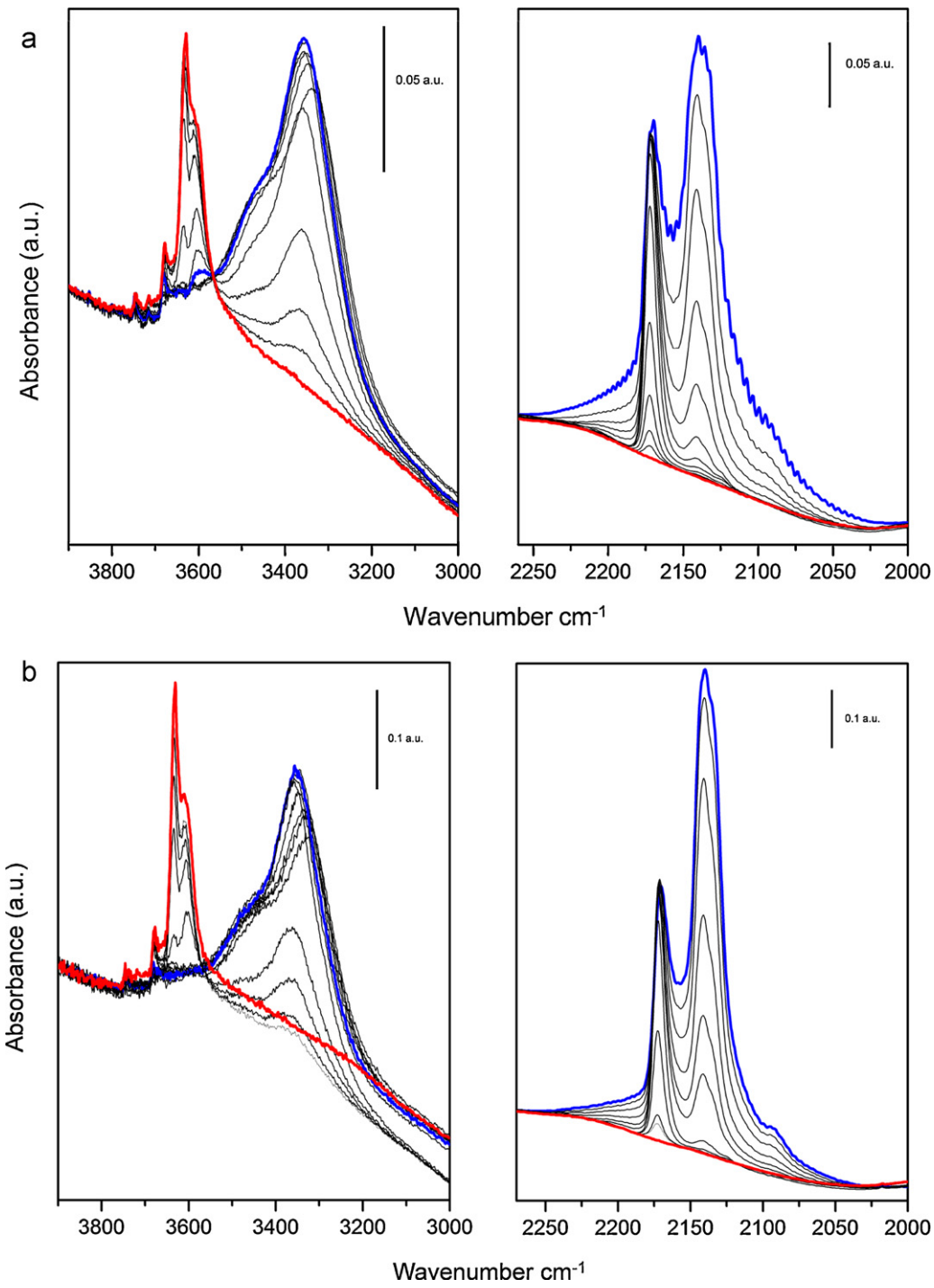

Fig. 5. Transmission infrared (IR) spectroscopy of the catalyst before (top) and after (bottom) 5 test – regeneration cycles at 400 °C and 550 °C, respectively. The OH stretch region is depicted on the left, while the CO stretch region is depicted on the right hand side. Red lines represent zero CO pressure, while blue lines represent maximum CO pressure, in the IR cell. (For interpretation of the references to color in this figure legend, the reader is referred to the web version of the article.)

Fig. S1. C_2 and C_3 species are the main products at both temperatures, as expected for this topology. Further, it is a general trend that the C_2/C_3 ratio increases with time on stream; more rapidly at the higher temperature, in line with the more rapid deactivation at this temperature (cf. Fig. 7), and with literature data [18].

The methyl chloride conversion capacity of the catalyst at the two temperatures was calculated by integrating the MeCl versus time on stream curves until the conversion had decreased to 10%. The conversion capacity was quite stable with increasing temperature, being 10.5 g MeCl/g cat at 350 °C and 11.0 g MeCl/g cat at 400 °C. It has previously been reported that the corresponding numbers for methanol conversion over H-SAPO-34 under similar conditions (albeit lower reactant partial pressure) was 7 and 23 g MeOH/g cat, respectively, at 350 and 400 °C [51]. Taking into account the higher molecular mass of methyl chloride compared to methanol, the conversion capacity of H-SAPO-34 was similar for the two at 350 °C (MeOH/MeCl conversion capacity ratio = 1.0), but much higher for methanol at 400 °C (MeOH/MeCl capacity ratio = 3.3), on molar basis.

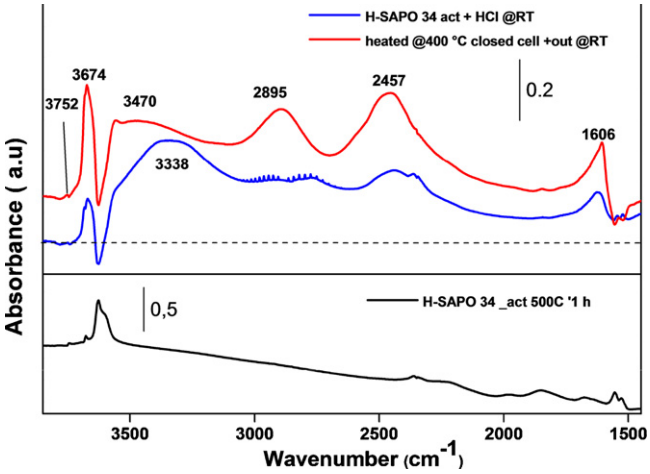

Fig. 6. Infrared spectra of H-SAPO-34 before (bottom) and after (top) treatment by HCl. The blue curve represents the samples after HCl treatment at room temperature (RT) and subsequent outgassing, while the red curve represents the samples after HCl treatment at RT followed by heating to 400 °C, cooling to RT and subsequent outgassing. (For interpretation of the references to color in this figure legend, the reader is referred to the web version of the article.)

3.4. Regeneration tests

Regeneration tests were performed to elucidate whether the possible acid site deterioration by HCl, as suggested by the findings in Section 3.2, would influence the long-term stability of the H-SAPO-34 material.

The resistance of H-SAPO-34 towards reaction and regeneration atmospheres was studied by subjecting it to 5 cycles of methyl chloride conversion at 400 °C, with intermediate regeneration in 10% O_2 in Ar for 16 h at 550 °C. A similar regeneration study has previously been reported [18]. However, at that time the fresh and used catalysts were only characterised by XRD, while in this study, the fresh and regenerated catalysts were also studied by IR, in order to elucidate possible changes in the Brønsted acid sites during testing and regeneration.

Conversion versus time on stream curves are shown in Fig. 8. The conversion curves for the 5 test cycles are mainly superimposed, except for the first two analyses, where a slight conversion decrease is observed from one cycle to the next. Integration of the

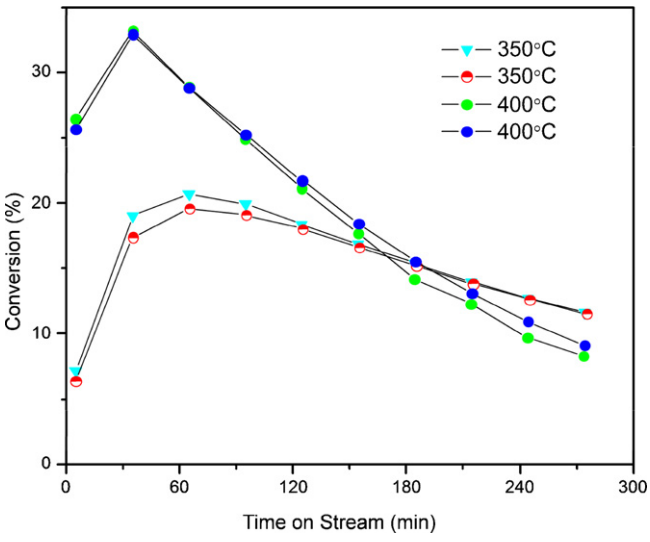

Fig. 7. MeCl conversion versus time on stream for H-SAPO-34 at 350 and 400 °C. P(MeCl) = 0.65 atm, WHSV = 11.7 h^{-1}. Two tests are reported at each temperature.

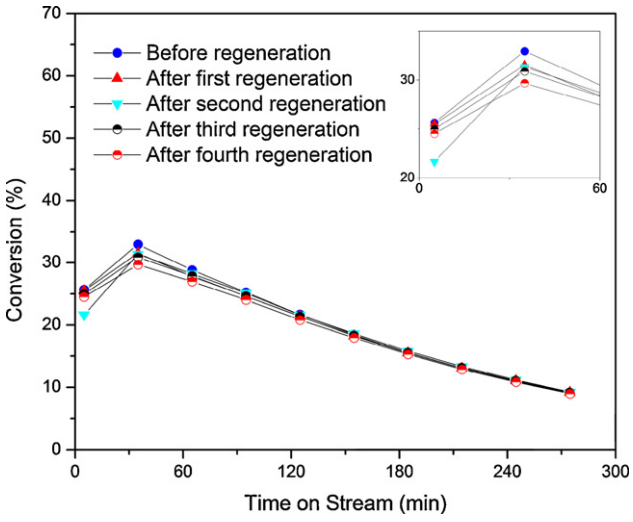

Fig. 8. MeCl conversion versus time on stream at 400 °C, P(MeCl) = 0.65 atm, WHSV = 11.7 h^{-1}, before and after testing and regeneration in air at 550 °C, 16 h.

conversion curves until 10% conversion was reached, gave a negligible decrease in conversion capacity from 11.0 g MeCl/g cat for the first cycle, to 10.6 g MeCl/g cat for the last cycle. This result indicates that H-SAPO-34 is resistant to the chlorine-containing atmosphere as well as the regeneration conditions. Product selectivities during the 5 test cycles are shown in Supporting information, Fig. S2. The product selectivities are very similar during each test cycle; the only exception being a minor increase in ethene and propene selectivity (from 29 to 32% and 42 to 44%, respectively) at the expense of C_5 selectivity during the fifth test cycle.

XRD and IR data for the fresh and used catalysts are shown in Figs. 3 and 5, respectively. The X-Ray diffraction data in Fig. 3 shows no degradation of the crystalline lattice during testing and regeneration, but a slight decrease in the signal-to-background ratio after testing may indicate the presence of an amorphous phase. The infrared spectra in Fig. 5 shows no significant changes between the fresh and used sample, after 5 test-regeneration cycles: No indication of Lewis acidity or silanol nest formation, which might arise from lattice desilication or dealumination during testing and/or regeneration, is observed. Neither is there any increase in the P–OH bond, which might be expected from interaction with HCl (see Section 3.2).

Su et al. have previously demonstrated the formation of P–OH species in H-SAPO-34 by in situ IR studies during CH_3Cl or CD_3Cl conversion over H-SAPO-34 at 350–400 °C [17]. Formation of such species was further evidenced by HCl adsorption in the present study (Fig. 6). When no such species is present after repeated test-regeneration cycles at 400 °C, it suggests that the bond breaking is fully reversible, and, furthermore, that the partial extra framework Al–Cl species which are formed simultaneously, have low mobility. In the CO stretch frequency range (Fig. 5, right), a slight decrease in the relative intensity of the peak assigned to CO interacting with strong Brønsted sites (2170 cm^{-1}) and the peak assigned to condensed CO (2140 cm^{-1}) is observed from the fresh (Fig. 5a) to the used (Fig. 5b) sample, respectively. However, this change may be due to the presence of quartz diluent in the catalytic experiment, and thus in the used sample.

3.5. Transient isotopic labelling experiments

Transient isotopic labelling experiments will generally provide information about major reaction intermediates in a sequential reaction scheme, since such intermediates will more rapidly implement the isotopically labelled component compared to products

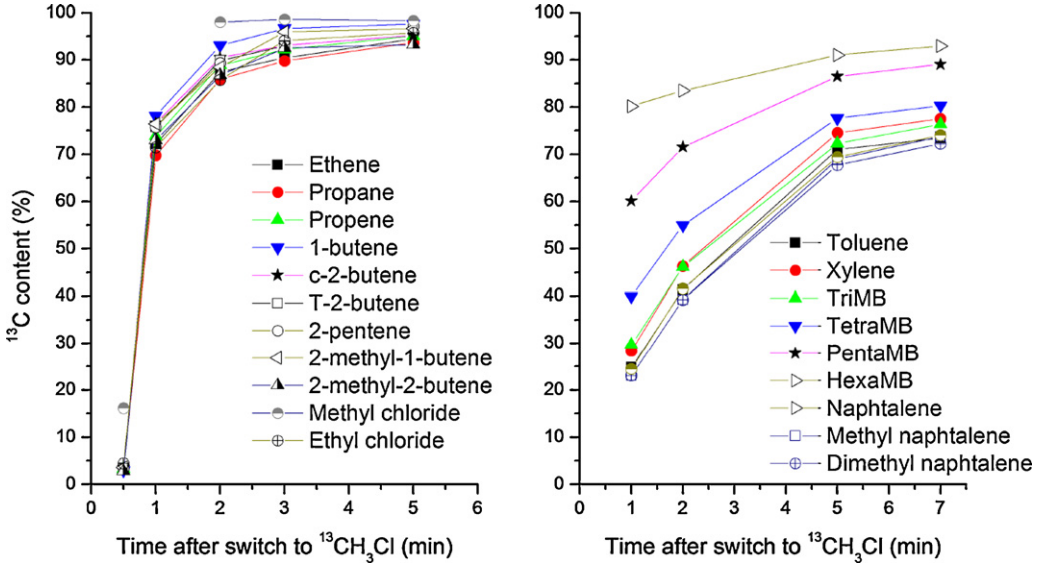

Fig. 9. ^{13}C content in effluent (left) and retained (right) reactant and products versus time after switching from a ^{12}C-MeCl feed to a ^{13}C-MeCl feed at 400 °C, P(MeCl) = 0.65 atm, WHSV = 11.7 h^{-1}.

formed later in the sequence, as well as products being inert towards further conversion. The aim of the experiments was to elucidate whether the reaction mechanism, as well as the main reaction intermediates, are the same in the MeXTO process as in the similar MTO process.

Transient isotopic labelling experiments were performed at 400 °C, with switching from ^{12}C-methanol to ^{13}C-methanol after 13 min on stream, when the catalyst was at its peak activity (cf. Fig. 7). The ^{13}C content in reactant and effluent products versus time after switching from ^{12}C-MeCl to ^{13}C-MeCl is shown in Fig. 9 (left) and corresponding curves for retained hydrocarbons in the catalyst are shown in Fig. 9 (right). The ^{13}C distribution within each product (not shown) was close to a random distribution at all times after switching, albeit with slightly enhanced zero-^{13}C and all-^{13}C product fractions.

Due to the low feed rate, only modest exchange of the reactant (17% ^{13}C) was observed 30 s after the switch. However, 2 min after the switch, MeCl consisted almost exclusively of ^{13}C (98% ^{13}C). At this time, the ^{13}C content of the effluent products (C_2–C_5 alkenes and alkanes) was in the range 85–93% ^{13}C. Five minutes after the switch all effluent products contained more than 90% ^{13}C. Throughout the sequence, the C_4^+ products contained the highest fraction of ^{13}C, and one may speculate that these products were formed either outside or at the periphery of the H-SAPO-34 crystals. Especially the branched C_5 alkenes cannot escape from the cavities of this topology, due to the narrow window dimensions.

The retained hydrocarbons consisted mainly of polymethylated benzenes (polyMB), and some polymethylated naphtalenes (polyMN). Among the retained hydrocarbons, hexaMB contained the highest fraction of ^{13}C at all times after switching (Fig. 9, right). At each measuring point, the ^{13}C content of the polyMBs decreased with a decreasing number of methyl groups on the benzene ring. This finding is in line with previous studies of the mechanism of the methanol to olefins reaction over the same topology [27,28,41]. The polyMNs contained even less ^{13}C than the lightest polyMBs. It is interesting to note that hexaMB contained a similar or higher ^{13}C fraction compared to the alkenes 1–5 min after switching. This observation suggests that hexaMB is an important reaction intermediate in alkene formation. The same conclusion has previously been reached for the MTO reaction over H-SAPO-34 catalyst [41].

3.6. Alkene co-feed experiments

It has previously been suggested that alkene products formed during the MeXTO reaction might inhibit MeCl conversion by competitive adsorption at acid sites [18]. To verify or disprove this hypothesis, alkene co-feed experiments were performed with isotopically labelled methyl chloride, and unlabelled alkenes, in order to distinguish products formed from either of them.

Experiments were performed at 400 °C, with WHSV = 11.7 h^{-1} for methyl chloride, and with a 1:1 carbon ratio between MeCl (^{13}C-labelled) and the alkene co-reactant (either ethene or propene; both ^{12}C). The methyl chloride conversion obtained during the ethene co-feed experiment was 28%, while the net conversion of ethene was 33%, after 5 minutes on stream. The corresponding numbers for the propene co-feed experiment was 35% methyl chloride conversion, and 66% net propene conversion, after 5 min on stream. Together, these data suggest that the alkenes do not inhibit methyl chloride conversion, which is in both cases similar to the optimum MeCl conversion observed without alkene co-feed (Fig. 7). Furthermore, the conversion of the alkene component is significantly higher than for methyl chloride, especially for propene which has the highest proton affinity among the three (647 kJ/mol for MeCl, 681 kJ/mol for ethene and 752 kJ/mol for propene [42]). This result suggests that there is a direct correlation between proton affinity and rate of conversion, and furthermore, that the coverage of acid sites on the catalyst was low during the experiments reported here, leading to insignificant competition for the active sites between the reactants.

Isotopic labelling fractions in the various products are shown in Fig. 10 for the ethene co-feed experiment. The ^{13}C distribution within each effluent product (not shown) was close to a random distribution, with a slight enrichment of zero-^{13}C and all-^{13}C product fractions. As expected, ethene had a low ^{13}C content (<10%). Ethyl chloride had similar ^{13}C content to ethene, and is probably an equilibrium product between ethene and HCl, as suggested previously [18]. Among the remaining reaction products in the effluent, the C_4^+ alkenes contained approximately 50% ^{13}C, which is in agreement with the similar conversion levels of ^{13}C-MeCl and ^{12}C-ethene, respectively. The ^{13}C content of propene, and especially propane, were slightly lower than for the other effluent products; the ^{13}C content of propane being very close to the 33% ^{13}C content expected

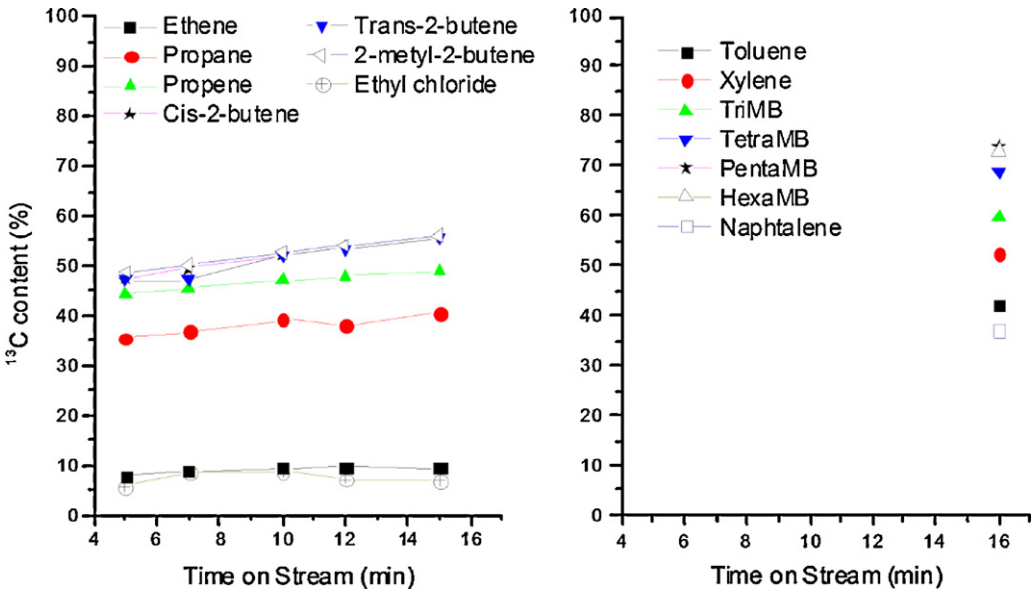

Fig. 10. ^{13}C content in effluent (left) and retained (right) reactant and products versus time during ^{13}C-MeCl and ^{12}C-ethene co-feed experiment at 400 °C, ^{13}C:^{12}C = 1:1, P(MeCl) = 0.50 atm, WHSV(MeCl) = 11.7 h^{-1}.

for direct ethene methylation by methyl chloride. It is interesting to note that the ^{13}C content of the retained hydrocarbons (polyMBs and MNs) is ≥35%, i.e. higher than the expected ^{13}C content of propene formed by direct ethene methylation (33%). The ^{13}C content increases with an increasing number of methyl groups on the benzene ring, to 75% ^{13}C for penta- and hexaMB. This result agrees well with a reaction mechanism in which aromatic rings are formed from alkenes (possibly starting with propene), and subsequently methylated by methyl chloride to the higher analogues, which are main intermediates for alkene formation in the MeXTO reaction, as suggested by the transient isotopic labelling experiments in Section 3.5.

Isotopic labelling fractions in effluent and retained products from the ^{13}C-MeCl/^{12}C-propene co-feed experiment are shown in Fig. 11. The ^{13}C content of the effluent products was lower than for the ethene co-feed experiment, in line with the higher conversion of propene compared to methyl chloride (66% versus 35%). The ^{13}C content of C_4^+ products were very similar (25–33%, increasing with time on stream), while the ^{13}C content of propyl chloride followed that of propene (20–14%, decreasing with time on stream). The ^{13}C content of ethene differed from the other alkenes, and was much higher (60–70%). This result suggests that ethene is mainly formed by another pathway than the other alkene products, and that methyl chloride is a dominating source of ethene. Previous studies of the methanol to hydrocarbons reaction over H-ZSM-5 catalysts have indicated that ethene is mainly formed from polymethyl benzene intermediates, while C_3^+ alkenes are mainly formed by alkene methylation and cracking, over that topology [53,54]. The isotopic labelling data obtained in the present study may suggest that the alkene methylation–cracking route is an important contributor to

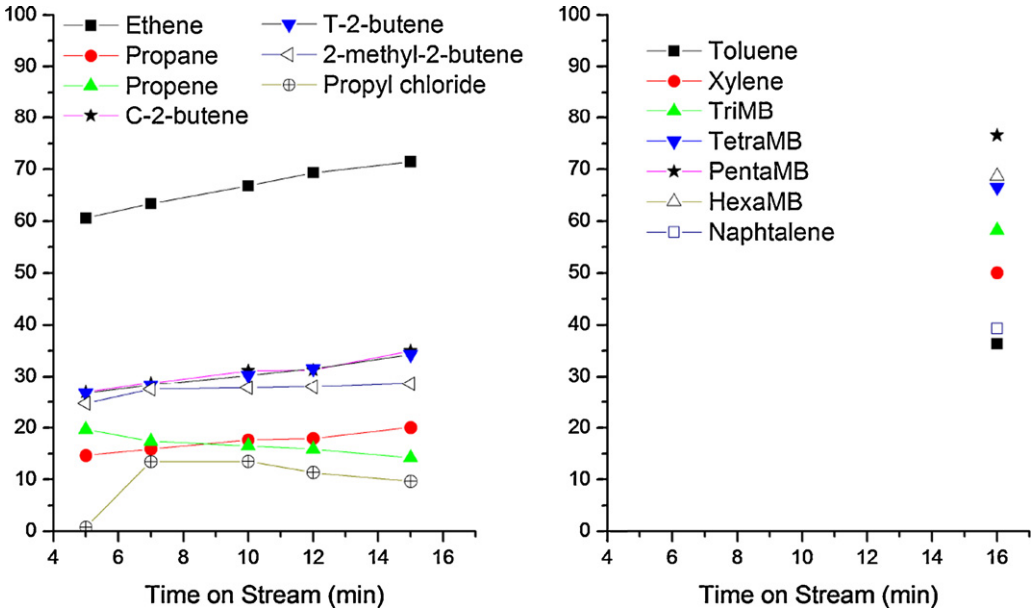

Fig. 11. ^{13}C content in effluent (left) and retained (right) reactant and products versus time during ^{13}C-MeCl and ^{12}C-propene co-feed experiment at 400 °C, ^{13}C:^{12}C = 1:1, P(MeCl) = 0.55 atm, WHSV(MeCl) = 11.7 h^{-1}.

C_3^+ alkene formation in the methyl chloride to olefins reaction even in the CHA topology of H-SAPO-34, where polyMBs have previously been suggested to be dominating intermediates in alkene formation from methanol [27,28,41]. In order to compare the two reactants in more detail, the data obtained in this study for methyl chloride–alkene co-feed over H-SAPO-34, are compared to data previously reported by Dahl and Kolboe for methanol–alkene co-feed over H-SAPO-34 in Supporting information, Fig. S3 (ethene co-feed) and S-4 (propene co-feed). The ^{13}C content of the effluent products was significantly higher in the case of ^{13}C-methanol–^{12}C-alkene co-feed than for ^{13}C-MeCl–^{12}C-alkene co-feed experiments. This result is expected when taking into account the higher proton affinity of methanol compared to methyl chloride (754 kJ/mol versus 647 kJ/mol, respectively [42]). Furthermore, the ^{13}C content of ethene in the methanol–propene co-feed experiment in literature, was also significantly higher than for t-2-butene, in line with similar data obtained for the methyl chloride–propene co-feed experiment in this study. Together, these data may suggest that alkene interconversion reactions are important for C_3^+ alkene formation even in the CHA topology, with methanol as the reactant.

4. Discussion

The main aim of the present study was to elucidate kinetic and mechanistic differences between methyl chloride and methanol conversion to light olefins over H-SAPO-34 catalyst. Co-feed experiments using ^{13}C-MeCl and ^{12}C-alkenes (ethene, propene) indicated a direct correlation between proton affinity and reaction rate for the title reaction, and may explain the lower conversion rate observed for methyl chloride compared to methanol, as suggested by theory [43]. The transient isotopic experiments where ^{12}C-MeCl was switched to ^{13}C-MeCl, further indicated that hexaMB is a major reaction intermediate in the MeXTO reaction over H-SAPO-34 (X = Cl). This result is similar to what observed for the MTO process over the same topology, and indicates that the influence of proton affinity on the overall reaction rate is not a kinetic influence, but rather a thermodynamic influence, leading to a lower coverage of active sites in $MeCl_{ads}$ compared to $MeOH_{ads}$. The insignificant influence of alkene addition on MeCl conversion further suggests a low coverage of the active sites under the conditions used here.

The detrimental influence of HCl on the strong Brönsted acidic sites which are responsible for the catalytic activity of H-SAPO-34, further complicates the picture. Its influence on the initial conversion of MeCl depends on the rate of Si–O–Al bond breaking, which could not be determined neither from the present study, nor from literature reports [15,17], since the catalyst was in both cases exposed to HCl (or MeCl) at RT or elevated temperature, and then evacuated at RT before the infrared measurements. It is, however, highly probable that such bond rupture is responsible for the significantly lower conversion capacity observed for MeCl compared to MeOH, at 400 °C. The self-healing effect of the H-SAPO-34 lattice observed during regeneration at 550 °C bears promise that the MeXTO process may still be of commercial interest, albeit with a need for more frequent regeneration cycles than for the MTO process.

Acknowledgements

Mrs. Sharmala Aravinthan, UiO, is acknowledged for assistance with the isotopic labelling experiments. This publication forms a part of the inGAP Centre of Research-based Innovation, which receives financial support from the Norwegian Research Council under Contract No. 174893.

Appendix A. Supplementary data

Supplementary data associated with this article can be found, in the online version, at doi:10.1016/j.cattod.2011.04.020.

References

[1] IEA (International Energy Agency), Natural Gas Market Review, 2009.
[2] J.R. Rostrup-Nielsen, Steam reforming, in: H. Ertl, F. Knözinger, F. Schüth, J. Weitkamp (Eds.), Handbook of Heterogeneous Catalysis, 2nd ed., Wiley-VCH, Weinheim, 2008, pp. 2882–2904.
[3] D.J. Wilhelm, D.R. Simbeck, A.D. Karp, R.L. Dickenson, Fuel Process. Technol. 71 (1–3) (2001) 139–148.
[4] A. Holmen, Catal. Today 142 (2009) 2–8.
[5] B. Vora, J.Q. Chen, A. Bozzano, B. Glover, P. Barger, Catal. Today 141 (2009) 77–83.
[6] S.G. Podkolzin, E.E. Stangland, M.E. Jones, E. Peringer, J.A. Lercher, J. Am. Chem. Soc. 129 (2007) 2569–2576.
[7] E. Peringer, M. Salzinger, M. Hutt, A.A. Lemonidou, J.A. Lercher, Top. Catal. 52 (2009) 1220–1231.
[8] G.A. Olah, B. Gupta, M. Farina, J.D. Felberg, W.M. Ip, A. Husain, R. Karpeles, K. Lammertsma, A.K. Melhotra, N.J. Trivedi, J. Am. Chem. Soc. 107 (24) (1985) 7097–7105.
[9] V. Degirmenci, A. Yilmaz, D. Uner, Catal. Today 142 (2009) 30–33.
[10] I.M. Lorkovic, S. Sun, S. Gadewar, A. Breed, G.S. Macala, A. Sardar, S.E. Cross, J.H. Sherman, G.D. Stucky, P.C. Ford, J. Phys. Chem. A 110 (28) (2006) 8695–8700.
[11] C.E. Taylor, R.P. Noceti, R.R. Schehl, Stud. Surf. Sci. Catal. 36 (1998) 483–489.
[12] C.E. Taylor, R.P. Noceti, Proc. Int. Congr. Catal. 9th, vol. 2, 1988, pp. 990–997.
[13] C.E. Taylor, Stud. Surf. Sci. Catal. 130D (2000) 3633–3638.
[14] Y. Wei, D. Zhang, L. Xu, Z. Liu, B.L. Su, Catal. Today 106 (2005) 84–89.
[15] Y. Wei, D. Zhang, Z. Liu, B.L. Su, J. Catal. 238 (2006) 46–57.
[16] Y. Wei, D. Zhang, Y. He, L. Xu, Y. Yang, B.L. Su, Z. Liu, Catal. Lett. 114 (2007) 30–35.
[17] Y. Wei, D. Zhang, Z. Liu, B.L. Su, Chem. Phys. Lett. 444 (2007) 197–201.
[18] S. Svelle, S. Aravinthan, M. Bjørgen, K.-P. Lillerud, S. Kolboe, I.M. Dahl, U. Olsbye, J. Catal. 241 (2006) 243–254.
[19] M.H. Nilsen, S. Svelle, S. Aravinthan, U. Olsbye, Appl. Catal. A: Gen. 367 (2009) 23–31.
[20] C.D. Chang, A.J. Silvestri, J. Catal. 47 (1977) 249–259.
[21] I.M. Dahl, S. Kolboe, Catal. Lett. 20 (1993) 329–336.
[22] I.M. Dahl, S. Kolboe, J. Catal. 149 (1994) 458–464.
[23] I.M. Dahl, S. Kolboe, J. Catal. 161 (1996) 304–309.
[24] P.W. Goguen, T. Xu, D.H. Barich, T.W. Skloss, W. Song, Z. Wang, J.B. Nicholas, J.F. Haw, J. Am. Chem. Soc. 120 (1998) 2650.
[25] Ø. Mikkelsen, P.O. Rønning, S. Kolboe, Micropor. Mesopor. Mater. 40 (2000) 95–113.
[26] W. Song, J.F. Haw, J.B. Nicholas, C.S. Heneghan, J. Am. Chem. Soc. 122 (2000) 10726–10727.
[27] B. Arstad, S. Kolboe, J. Am. Chem. Soc. 123 (2001) 8137–8138.
[28] B. Arstad, S. Kolboe, Catal. Lett. 71 (2001) 209–212.
[29] A. Sassi, M.A. Wildman, H.J. Ahn, P. Prasad, J.B. Nicholas, J.F. Haw, J. Phys. Chem. B 106 (2002) 2294–2303.
[30] A. Sassi, M.A. Wildman, J.F. Haw, J. Phys. Chem. B 106 (2002) 8768–8773.
[31] M. Bjørgen, U. Olsbye, S. Kolboe, J. Catal. 215 (2003) 30–44.
[32] M. Bjørgen, F. Bonino, S. Kolboe, K.-P. Lillerud, A. Zecchina, S. Bordiga, J. Am. Chem. Soc. 125 (2003) 15863–15868.
[33] M. Seiler, W. Wang, A. Buchholz, M. Hunger, Catal. Lett. 88 (2003) 187–191.
[34] M. Bjørgen, U. Olsbye, S. Svelle, S. Kolboe, Catal. Lett. 93 (2004) 37–40.
[35] M. Bjørgen, U. Olsbye, D. Petersen, S. Kolboe, J. Catal. 221 (2004) 1–10.
[36] B. Arstad, J.B. Nicholas, J.F. Haw, J. Am. Chem. Soc. 126 (2004) 2991–3001.
[37] U. Olsbye, M. Bjørgen, S. Svelle, K.-P. Lillerud, S. Kolboe, Catal. Today 106 (2005) 108–111.
[38] S. Svelle, M. Bjørgen, S. Kolboe, D. Kuck, M. Letzel, U. Olsbye, O. Sekiguchi, E. Uggerud, Catal. Lett. 109 (2006) 25–35.
[39] W. Wang, Y. Jiang, M. Hunger, Catal. Today 113 (2006) 102–114.
[40] D.M. McCann, D. Lesthaeghe, P.W. Kletnieks, D.R. Guenther, M.J. Hayman, V. Van Speybroek, M. Waroquier, J.F. Haw, Angew. Chem. Int. Ed. 47 (2008) 5179–5182.
[41] B.P.C. Hereijgers, F. Bleken, M.H. Nilsen, S. Svelle, K.P. Lillerud, M. Bjørgen, B.M. Weckhuysen, U. Olsbye, J. Catal. 264 (1) (2009) 77–87.
[42] NIST Chemistry WebBook, http://webbook.nist.gov/chemistry/ (28.04.2009).
[43] F. Bleken, S. Svelle, K.P. Lillerud, U. Olsbye, B. Arstad, O. Swang, J. Phys. Chem. A 114 (2010) 7391–7397.
[44] B.M. Lok, C.A. Messina, R.L. Patton, R.T. Gajek, T.R. Cannan, E.M. Flanigen, US Patent 4,440,871 (1984) Example 35.
[45] I.M. Dahl, R. Wendelbo, A. Andersen, D. Akporiaye, H. Mostad, T. Fuglerud, Micropor. Mesopor. Mater. 29 (1999) 159–171.
[46] C. Paze, B. Civalleri, S. Bordiga, A. Zecchina, J. Phys. Chem. B 102 (1998) 10753–10764.
[47] C. Paze, S. Bordiga, G. Spoto, C. Lamberti, A. Zecchina, J. Chem. Soc., Faraday Trans. 94 (1998) 309–314.
[48] P.O. Rønning, Ph.D. Thesis, University of Oslo, 1998.

[49] S. Svelle, P.O. Rønning, S. Kolboe, J. Catal. 224 (2004) 115–123.
[50] P. Magnoux, P. Roger, C. Canaff, V. Fouche, N.S. Gnep, M. Guisnet, Stud. Surf. Sci. Catal. 34 (1987) 317.
[51] F. Bleken, M. Bjørgen, L. Palumbo, S. Bordiga, S. Svelle, K.P. Lillerud, U. Olsbye, Top. Catal. 52 (2009) 218–228.
[52] A. Zecchina, G. Spoto, S. Bordiga, Phys. Chem. Chem. Phys. 7 (2005) 1627–1642.
[53] S. Svelle, F. Joensen, J. Nerlov, U. Olsbye, K.P. Lillerud, S. Kolboe, M. Bjorgen, J. Am. Chem. Soc. 128 (2006) 14770–14771.
[54] M. Bjørgen, S. Svelle, F. Joensen, J. Nerlov, S. Kolboe, F. Bonino, L. Palumbo, S. Bordiga, U. Olsbye, J. Catal. 249 (2007) 195–207.